Metamaterials for Space Applications

Cloaking via a full dielectric metamaterial and transformation optics for high resolution focusing

Final Report

Authors: D. P. Gaillot, C. Croënne and D. Lippens
Affiliation: Institut d'Electronique de Microélectronique et de Nanotechnologie, Université des Sciences et Technologies de Lille

ESA Researcher(s): Jose M. Llorens and Luzi Bergamin

Date: 11.7.2008

Contacts:

Didier Lippens
Tel: + 33 3 20 19 78 77
Fax: + 33 3 20 19 78 92
e-mail: didier.lippens@iemn.univ-lille1.fr

Leopold Summerer
Tel: +31(0)715655174
Fax: +31(0)715658018
e-mail: act@esa.int

Available on the ACT website
http://www.esa.int/act

Ariadna ID: 07/7001c
Study Duration: 4 months
Contract Number: 21260/07/NL/CB

Abstract

We report on two important applications in connection with transformation optics. The first one concerns the application to invisibility cloaks. With respect to the various solutions reported in the literature, based on effective permeability or permittivity gradients, the originality here stems from the introduction of a new technology based on magnetic Mie resonance which can be found in high-κ ceramics. The possibility to induce such an artificial magnetization is first of all demonstrated experimentally via scattering parameters measurements on Barium Strontium Titanate Ceramic ferroelectric cubes. We then address one of the key issues of cloaking devices, namely the frequency dependence of their performance which is here studied via the calculation of the radar cross section. An extreme sensitivity to the dispersion of the effective parameters and to the size of the cloak is pointed out. The second application, which was considered in this Ariadna study, concerns transformation optics for achieving magnification and high resolution in hyperlenses. Let us remind that the hyperlens concept is based on a channeling effect in highly anisotropic media and was recently demonstrated experimentally by using multilayered metal-dielectric microstructures deposited onto a curved groove. The original result of the present study in this field is to show that magnification effects, with a limited spreading in space, can be achieved in flat hyperlens by taking benefit of channelling effects in highly anisotropic layered media.

Contents

1 Introduction

The moulding of the flow of light was already the main goal of the photonic crystal technology [2]. Towards this goal, new degrees of freedom were afforded by the emergence of the so-called metamaterial technology based on the structuring of artificial matter on a scale much shorter than the operating wavelength. This permits one to open the effective parameter space with not only negative values of the effective permittivity and permeability but also the possibility to consider zero index media or having permittivity and permeability values which vary between zero and one. This latter case corresponds to a superluminal operating condition and hence allows the bending of light in certain regions of the geometrical space by keeping the same time of flight with respect to the corresponding straightforward transmitted waves. The Fermat principle is hence satisfied.

Such a bending of light opens the way to electromagnetically isolate some regions of space which thus become undetectable by a point or distributed probing source. Any scatterers such as a metal rod or sphere, depending of the dimensionality of the system, placed in these isolated space regions, becomes invisible or equivalently becomes "transparent" for the probing waves. Figure 1 illustrates how the device diverts the flow of the impinging light around the concealed region. The activity in this research field, termed cloaking, is now mainly concentrated in the design, fabrication, and experimental assessment of invisibility cloaks. The references [3, 9] can be considered as the seminal papers in the very recent field which revisits the invisibility concept.

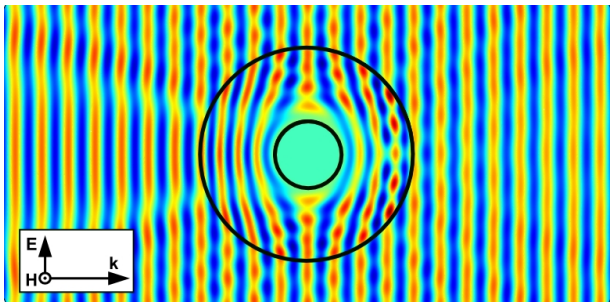

Figure 1: Normal component of the light magnetic field scattered by an invisibility cloak.

So far, most of the experimental works which were reported for achieving such a high degree of transparency use the idea of space deformation by means of gradient index cloaks. In the microwave spectral region, the index gradients are mainly achieved by an engineering of the effective permeability. Now, it is well known that current metal loops, which can be compared to the so-called split ring resonator technology, yield negative values of the effective permeability between the resonant and the plasma magnetic frequencies. Above the magnetic plasma frequency, the value of μ_{eff} can thus be comprised between zero and one. In optics, the engineering of the effective permittivity was found preferable and some modelling results have been published on ellipsoidal-shaped radial metal inclusion [7] or non uniform section bars, in order to induce permittivity gradients. With respect to the first principle experimental demonstrations, a microwave cloak was recently realized [6]. It was based on a reduced set of equations (see Ref. [8]) for relaxing the technological difficulty since an ideal cloak approach requires engineering simultaneously the permittivity and permeability parameters. In practice, the cloak was

made of concentric dielectric cylindrical-shaped boards with printed edge-coupled C-shaped split ring resonators.

However, targeting higher frequencies, notably the Terahertz spectral region by shrinking the SRR dimensions, appears problematic. The reason is the complexity of the realization of such a prototype whose dimensions have to be on a micron-scale. The terahertz spectral range is of critical relevance for space science. Astronomical THz spectroscopy or milimeter, submilimeter and far-infrared spectroscopy, as it is better known in that community, plays a key role in the chemical analysis of interstellar, stellar and planetary environments [1]. In this paper, we show how operation at higher frequencies can be achieved by taking advantage of the ground magnetic Mie resonance in high-κ dielectric rods. Recently, we showed that the basic principle is similar to that of used in SRR, namely an engineering of the magnetic response by size-effects [10]. Here it is shown that the operating frequency can be extended by more than two orders of magnitude with similar prospect in terms of performances. In a more general manner, we also address the problem of the size of the object that we would like to cloak.

On the other hand, transformation optics can be applied to many applications including high resolution focusing. Among the various possibilities reported in the literature special attention was paid here on the concept of hyperlens whose basic concept was published simultaneously in Refs [11, 12]. The hyperlens is a subwavelength imaging device, able to form the image of an object whose dimension lay below the diffraction limit. Its working principle consists in transforming the non-propagation modes generated by an extended source into propagation ones. An experimental demonstration was published recently in [13, 14] where they reported the fabrication of a multilayered metal-dielectric microstructure deposited on a curve-etched substrate. In addition, the multilayered stack corresponds to a highly anisotropic system with in-plane values of the permittivity tensor close to zero. It results from this a magnification effect without spreading of the propagating beam which can be used to improve the resolution of an imaging system which operates in the far field. Our contribution in this research field will be to see whether the requirement of a deposition on pre-etched surface can be avoided by keeping the condition of a highly anisotropic medium. Thus, we demonstrate that a magnification can be achieved with a flat hyperlens. At last, we report on the preliminary development of an extension of this work to the high resolution focusing system. In Section 2 we describe the details of the invisibility cloak under study. Section 3 deals with the experimental demonstration of artificial magnetism in High-κ ferroelectric ceramics, the metamaterial we chose for the realization of the device. On this basis, we address in section 4 the cloaking issues by considering small size and large size cloaked objects. In section 5 , the application of transformation optics rules to the synthesis of a flat hyperlens and to a high resolution focusing system is presented while conclusions and prospect are given in section 6.

From the point of view of space applications many systems on board of a spacecraft can exploit the transformation optics features by enhancing its performance. In particular the invisibility devices provide not only a way to control the flow of light but also the solar pressure associated to it. In the same way new radiation shielding proposals can be envisaged.

2 Cloak design

We pursue the design of a cylindrical cloak defined by its inner radius a and outer radius b, the effective parameters of the cloak shell (permittivity and permeability) must be independently engineered to satisfy a set of equations derived from the conformal transformation theory [5]. On the other hand, it was shown that this design burden can be overcome by using a reduced set of equations [8]. This allows one parameter only (permittivity or permeability) to be varied with the cloak radius. Under this configuration, a transverse-electric (TE) polarized plane wave (H_r, H_θ, E_z in cylindrical coordinates) has to be employed to illuminate the magnetic cloak and the original set of equations can be reduced to:

$$\mu_r(r) = \left(\frac{r-a}{r}\right)^2, \tag{1}$$

$$\mu_\theta(r) = 1, \tag{2}$$

$$\varepsilon_z(r) = \left(\frac{b}{b-a}\right)^2. \tag{3}$$

Only μ_r is required to be inhomogeneous. The only feasible way to obtain such behaviour is by means of a metamaterial. In this work we use ferroelectric rods made of BST, in which magnetic resonances are induced modifying its value of the permeability. The origin of such effect rely on Mie resonances which depend on the geometry of the scatterer. Therefore the inhomogeneous profile of μ_r is be obtained by positioning of BST rods of different size. Before entering in the discussion of the cloak performance we will review some fundamentals of the Mie magnetic resonances.

3 Basic principle of Mie magnetic resonance

The basic principle for the achievement of a magnetic dipole by using high dielectric rods can be understood by considering Fig. 2. This Figure shows the displacement current in an infinite dielectric rod whose complex permittivity value is ε= 200+5i with a polarization of the magnetic field parallel to the rods. This typical value of permittivity was chosen in the seminal paper published by O'Brien and Pendry on this topic [15]. On the other hand, the values chosen here are representative of the present ferroelectrics technology notably with respect to the Barium Strontium Titanate (BST) material system for which the real part of the permittivity exceeds 100 whereas the loss tangent can be maintained at values close to 10^{-2}. The large values of the permittivity with respect to the embedding medium (air) insure a high confinement of the electromagnetic wave on a scale much lower than the wavelength. As a consequence, the metamaterial condition can be met despite the fact that we are considering a full dielectric route. The induced circular displacement current induces a magnetic response which can be out of phase (negative value of the permeability) above the resonant frequency. When the rods are organized in arrays, which is the case in the simulation with appropriate boundary condition in order to mimic an infinite medium, the negative permeability is lost above the magnetic plasma frequency.

These considerations can be quantitatively assessed by means of the retrieval of the effective permeability which is plotted in Fig. 2(b) as a function of the normalized frequency

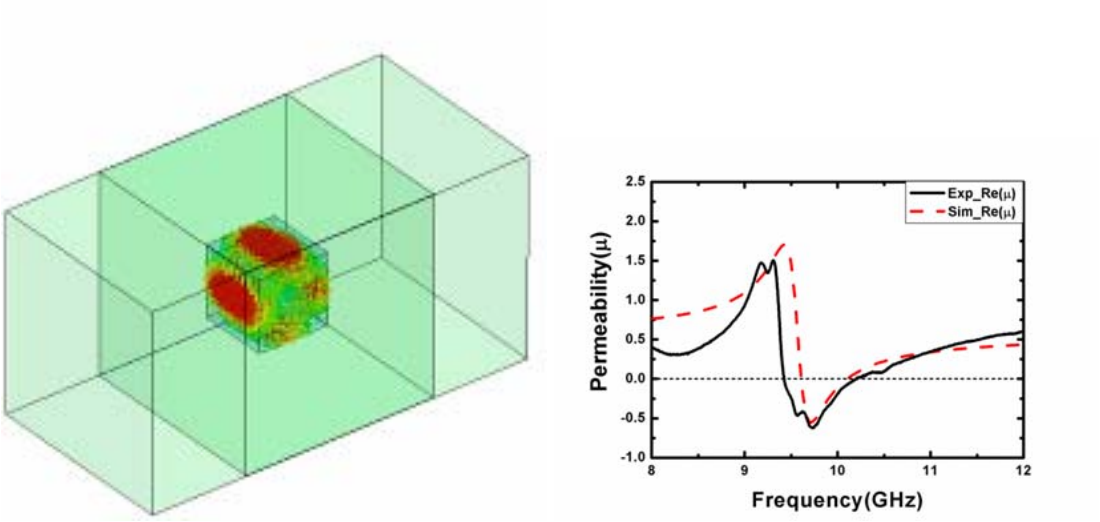

(a) (b)

Figure 2: (a) Map of the displacement current flowing circularly in the high-κ rod. (b) Dispersion of the effective permeability.

$f_{\text{operating}}/f_{\text{resonance}}$. The frequency dependence of the effective permeability follows a Lorentz-type dispersion characteristic with negative values of the permeability between the resonant frequency and the magnetic plasma frequency. Both frequencies can be engineered in the same way as with split ring resonators. In fact, we learnt from the analysis outlined above that the basic principle at the origin of an artificial magnetic moment is similar with respect to SRR physics. Therefore, the same engineering rules can be applied to tailor the resonant frequency and the magnetic plasma frequency which depend on the filling factor. As a consequence, two degrees of freedom can be defined with the radius of the rods and the array period. As demonstrated in ref. [10] for cloaking, this would be the values of μ_{eff} above the plasma frequency which will be of interest with the radial variation of the rod radius whereas the period is kept constant. Before considering in more details the advantages but also the drawbacks associated to such a full dielectric cloak, we report hereafter some experimental verification that a bulk ferroelectrics technology is suitable for inducing an artificial magnetic response. This experimental demonstration will be carried out at microwave for sake of simplicity. However, the underlying principles are valid over a large portion of the electromagnetic spectrum provided that a high value of permittivity can be preserved. While a cylinder-shaped rod is ideal for achieving circular currents, their fabrication in practice is troublesome at ultra-small dimensions. Recently, the University of Tsinghua succeeded to fabricate BST ceramic cubes which were subsequently characterized over a wide temperature range around the Curie temperature [16] One can find in this reference further details about the fabrication techniques and the temperature dependence of the material properties. Here, special attention will be paid to the experimental derivation of the dispersion characteristics at room temperature. To this aim, BST ceramic cubes were organized into a square lattice embedded into a Teflon film as shown in the photo of Fig. 3. The side of the cube is 0.9 mm for a permittivity value as high as 850. Under this condition, it can be shown that the resonant frequency lies in the X-band (8-12 GHz). The BST unit cell size fulfils the metamaterial condition as it can be verified from Fig. 3(a). The dominant mode in

the rectangular hollow waveguide is a TE_{10} mode with half a wavelength over the aperture of the flange. Figure 3(b) shows the variation versus frequency of the magnitude of the scattering parameter S_{21} which was measured by vectorial network analysis and calculated by means of a full wave analysis (commercial software High Frequency Simulator by Ansoft). As expected, at the resonant frequency here around 9 GHz the frequency dependence S_{21} shows a dip in the transmission showing that the one cell layer can be compared to a single negative medium.

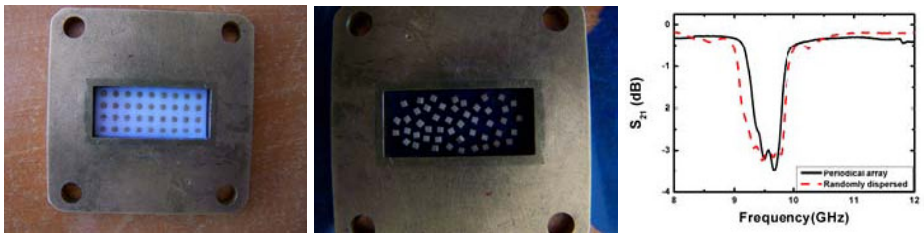

(a) (b) (c)

Figure 3: Photo of high-κ ceramic BST (Barium Strontium Titanate) cubes (periodic and random scheme) Courtesy of the University of Tsinghua [16] and illustration of the Mie magnetic resonance.

Further information about the dispersion of the effective parameters can be achieved by means of retrieval techniques. Figure 4 shows the results extracted by means of a Fresnel inversion technique. Similar results are obtained by using a field summation technique [17] which was used in our previous publication on cloaking. It can be seen that above the resonant frequency the one-cell layer exhibits a negative permeability whereas the effective permittivity is almost constant with an effective value close to 1.7.

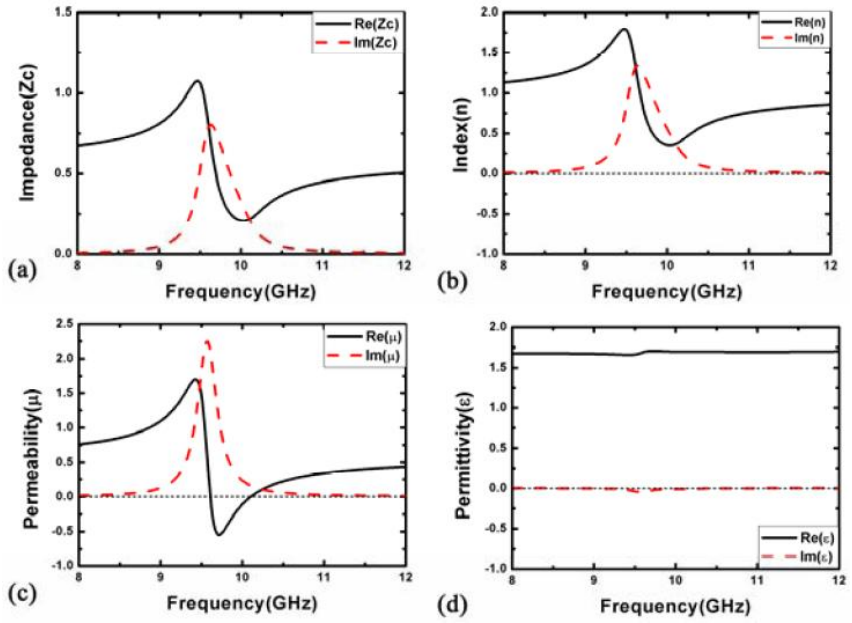

Figure 4: Retrieval of the complex impedance (a), propagation constant (b), and the corresponding effective magnetic permeability (c) and electric permittivity (d).

4 High-κ ceramic electromagnetic cloak at terahertz frequencies

As outlined in the introduction, the main advantage of a BST cloak is the simplicity of fabrication in the Terahertz range. Also, one can imagine to extend further the operating frequency up to the mid- and near-infrared spectral region. However, the main difficulty towards this goal stems from the fact that the BST cube exhibits Debye relaxation effects. It becomes more and more difficult to preserve high permittivity values and, as a consequence, to fulfil the metamaterial condition resulting of a high confinement on a sub-wavelength scale. Let us now consider above for cloaking. Figure 5 summarizes the main features of a 3D cloak with the rod arrangement, and the mapping of the E-field magnitude for an infinite conductivity metal cylinder with and without the cloak. The calculations were here performed by describing all the details of the microstructure and not by considering a multilayered homogenous structure. In order to illustrate these ab-initio calculations, a zoom of the cloak region (Fig. 5(c)) was also displayed showing the localization of the electromagnetic fields on a sub-wavelength. These calculations were performed with a permittivity of the rods equal to ε= 200+5i and for an operating frequency around 0.5 THz. Further details on the reduced equations and the variation in the geometry of high-κ rods can be found in [10].

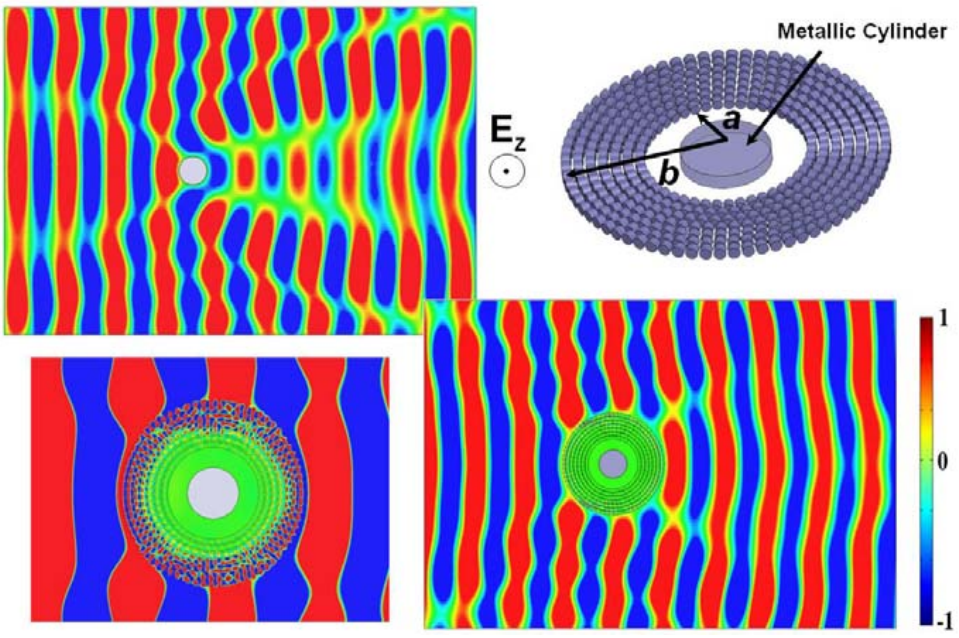

Figure 5: Steady-state E_z pattern calculated at 0.58 THz for a copper rod without (a) and with (d) a 3D microstructured cloak shown in (b). The plane of observation is located at mid-distance between the bottom and top face of the simulation domain. The wavefronts are well reconstructed behind the cloak without noticeable backscattering. The metallic particle placed at the center of the device is near "invisible" to a detector located at the output port. (c) Zoomed view of the field pattern within the cloak. For clarity, the amplitude within the cloak was magnified.

The mapping of the EM fields is a first stage in the assessment of an invisibility cloak.

However, the calculation of the radar cross section can bring further quantitative information about the sensitivity of the performance to the index gradients and also the cloaking bandwidth. In the following, we will apply this approach to the case of small size and large scale cloaks with respect to the wavelength of the incident wave. For this systematic study, we used an homogeneous multilayered description for saving computational time [8]. In other words, we break the continuous cloaking material into shells along the radial direction. For each shell, the effective parameters are those which can be computed by the field summation technique [17]. This technique whose results have been compared recently to the Fresnel inversion procedure is comparable to the averaging technique of Smith and Pendry [18]. In a first stage, it can be verified that the performance of a microstructured and of a multi-shell cloak are similar provided that the pitch determined by the number of discrete layers is small with respect to the wavelength. The main difference appears qualitatively on the field maps which show finer features in the space variations for a microstructured cloak. Let us first consider a small size cloak in the sense that the scatterer placed inside the cloak is of the order of the incident wavelength.

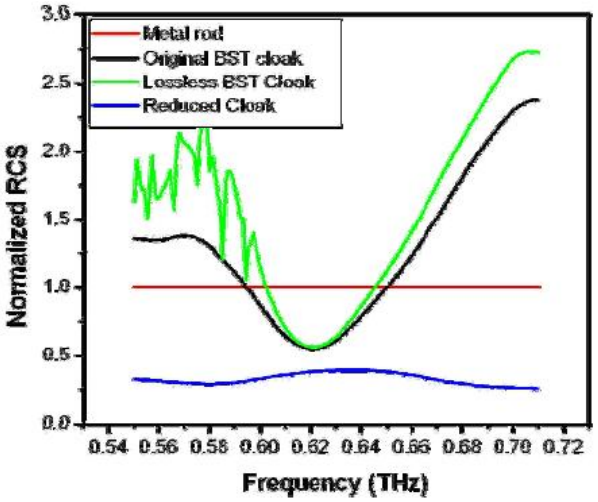

Figure 6: Total scattering cross-section normalized to the scattering cross-section of a bare metallic cylinder as a function of frequency for the bare metal cylinder (red), the reduced cloak (blue) and the lossless (green) and lossy (black) BST cloaks.

We first calculated the total radar cross section (RCS) of cylinder shaped perfect electric conductor then for a BST cloak and a reduced cloak. The latter is a single frequency cloak whose effective parameters can be found in ref. [8]. The scattered fields are calculated using the finite element solver COMSOL MULTIPHYSICS. By integrating the scattered field components in all directions, the RCS figure of merit can be deduced and results are presented in Fig. 6. With respect to the RCS of 100 % of a metal rod, it can be seen that introducing a non-dispersive cloak reduces the RCS to 30 %. This reduction is substantial but is still far from the invisibility criterion of an ideal cloak. However for a BST cloak, namely when we introduced dispersive effective parameters, this partial transparency exhibits a narrow band which can be estimated here of the order of 10 %. The fact that the frequency dependence of the effective permeability exhibits a Lorentz-type behaviour could explain such a narrow band [10]. A non-resonant feature obtained in a Drude-like dispersion characteristic would appear more

favourable in terms of bandwidth. However, with respect to these simple arguments, it has to be emphasized that we are far from the frequency range in which the metamaterial shows strong anomalous dispersion. Indeed, in this range the material exhibits considerable absorption close to the resonant frequency which counteracts the purpose of transparency. In any case, the losses impact the performance of the cloak in terms of RCS reduction and bandwidth. In Fig. 7 we show the dependence of the RCS spectrum on the cloak size, by varying the dimensions of the microwave cloak presented in Ref. [6]. In the vicinity of the cloaking frequency, the frequency behaviour between the various cases is similar except a narrowing of the bandwidth for larger cloacks. As a consequence, there is a trade-off between bandwidth and efficiency of the cloak which can be monitored also by a reasonable degree of losses notably when partial invisibility is sufficient. Let us now consider an oversized cloak with the following parameter characteristics ε_r=4, ε_θ=1, $\mu_r(r) = (1 - a/r)^2$. In order to maintain a reasonable number of layers the continuous variations of the reduced parameters were discretized into 20 shells for an inner radius of 3 mm which has to be compared to the wavelength at the operating frequency namely around 0.6 THz (a/λ_0=6).

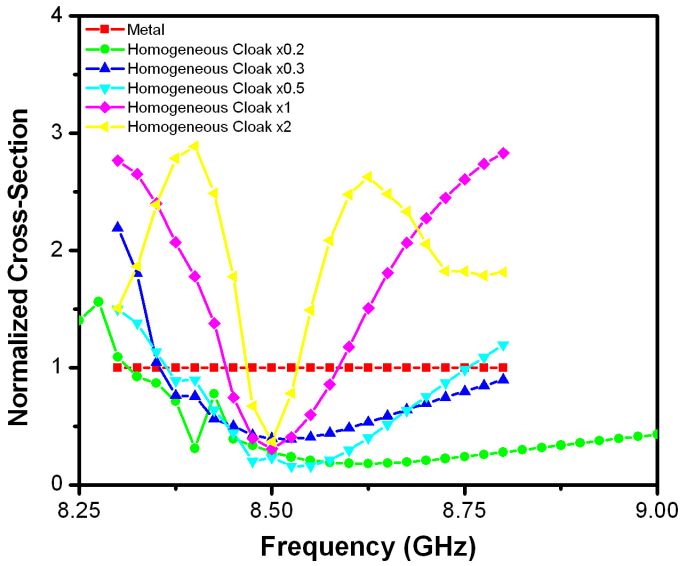

Figure 7: Frequency dependence of the Radar Cross Section for various cloak sizes.

Figure 8 illustrates the scattering patterns by the plot of the E-field component perpendicular to the 2D cloak (E_z) for a dispersion-less situation (reduced cloak) and when the dispersion of the BST material is taken into account. The corresponding frequency dependence of the normalized RCS with respect to the bare metal rod is also plotted. The fact that the reduced equation permits to lower the radar signature of a cloaked perfect electric conductor is here confirmed with a reduction of RCS down to 0.3-0.25. When the dispersion of the parameter is introduced in the simulation of this large cloak, it can be seen that the cloaking bandwidth is very narrow with a value close to 1 %. Therefore, very close to the vicinity of partial transparency frequency the efficiency of the cloak is rapidly degraded. This very high sensitivity of the

bandwidth to the size of the object located in the isolated region of space has to be confirmed by systematic simulation. However, it appears that this is not a specificity of a BST cloak because as aforementioned the dispersion characteristic are primarily responsible of the narrowing of the band.

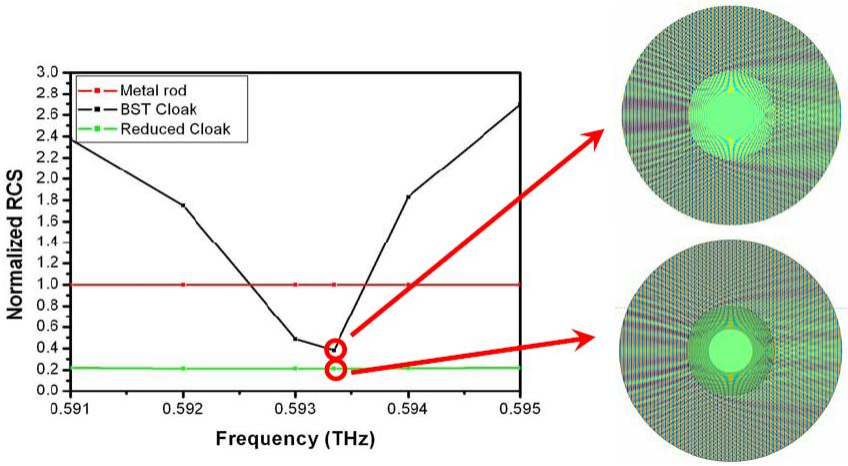

Figure 8: Variation versus frequency of the radar cross section for a metal rod (red) a reduced (green) and a BST oversized cloak (black).

5 Transformation Optics applied to magnification in flat hyperlens

The transformation procedure used to design a cloaking device is quite general [4]. In this section, we will use this technique to magnify near-field patterns. Such a function is performed by a class of devices termed hyperlenses [11, 12]. The main idea is to channel and magnify any near-field pattern in order to bring its fine details, originally carried by evanescent waves only, over the Abbe limit. Consequently, at the output of the hyperlens, those details are converted into propagating waves which can then be probed in the far-field by a conventional imaging system. The already existing hyperlens devices are based on a channeling effect which can be observed in highly anisotropic metamaterials when their transverse permittivity (for TM polarization) is positive and very close to zero. Such effective parameters can be obtained with nanostructures that alternate metallic and dielectric layers. The magnification effect is then obtained by means of a cylindrical conformation of the layers. In other words, this hyperlens maps the near-field patterns of a small inner cylinder onto a large outer one. The magnification coefficient is simply given by the ratio of the radii. One of the drawbacks of such a structure is that both interfaces are cylinders and, therefore, introduce an important limitation in the lateral extent of the input patterns. In the following, starting from the flat channeling device, we will add the magnification effect by means of transformation optics, while keeping both interfaces flat. Let us consider a flat channeling device in the XY plane; Z is the direction of the magnetic field (TM polarization) whereas Y is the main propagation direction. Consequently, we have to choose a very low value for ε_{xx}. In the following, we will use the lossless parameters (ε_{xx}, ε_{yy},

μ_{zz}) = (0.001, 2.5, 1). The device is positioned between $y = a$ and $y = b$. The magnification factor is t. The coordinate transformation used in the procedure is as follows:

$$x' = \left[\left(\frac{y-a}{b-a}\right)(t-1)+1\right]x\,, \tag{4}$$

$$y' = y\,, \tag{5}$$

$$z' = z\,. \tag{6}$$

This transformation is linear with respect to x and y. On the input interface (y = a), we have an identity between the original and the transformed coordinates. On the output interface (y = b), we "stretch" the coordinates along the x direction by a factor of t (x' = tx). It should be noted that such a transformation introduces an "optical axis" since the translation along x is proportional to the distance to $x = 0$ at the input. However, at this point, it is not necessary to limit the device along the x direction. By following the procedure presented in [5] for our linear transformation, we obtain the local expressions for both the 2×2 permittivity tensor $\bar{\bar{\varepsilon}}$ and the out-of-plane permeability (in our 2D TM case) of the device equivalent to the transformed space. Those expressions only depend on the position, on the geometrical parameters (a, b, t) and on the original material parameters (ε_{xx}, ε_{yy}, μ_{zz}). They are plotted in Fig. 9 for a=1 mm, b=5 mm and t=5, as an example.

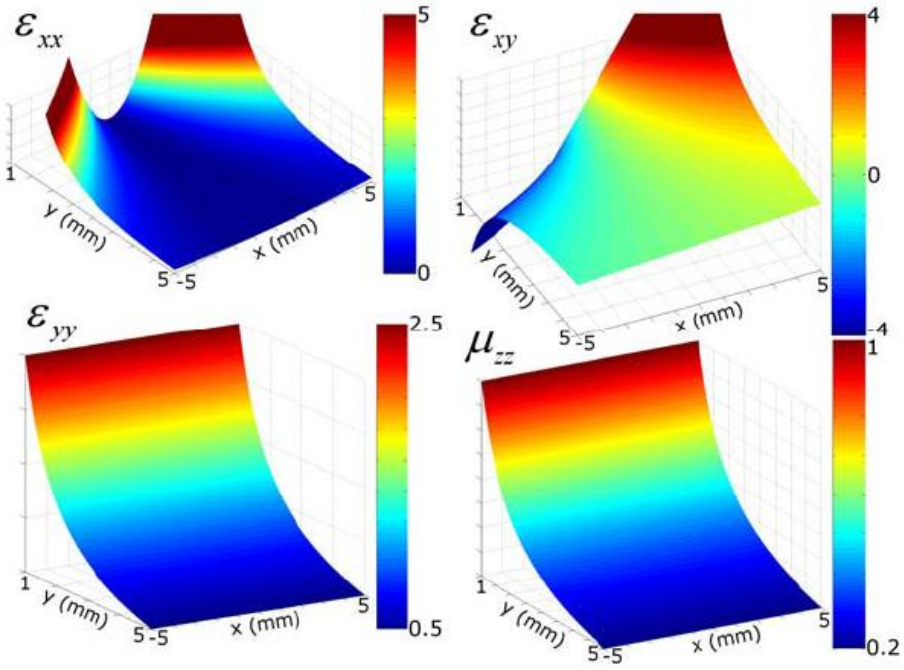

Figure 9: Full set of targeted effective parameters inside the flat hyperlens. Here, a=1 mm, b=5 mm and t=5 have been taken as an example. The values of y and ε_{xy} at the corners are off-scale.

The next step is to find whether we can avoid the off-diagonal term ε_{xy} in the permittivity tensor, which would be the most difficult to implement. This can be done by a proper local rotation $R(x, y)$ of angle $\theta(x, y)$ of the global cartesian coordinate system (x,y,z). We solve:

$$\begin{pmatrix} \varepsilon_{ii} & 0 \\ 0 & \varepsilon_{jj} \end{pmatrix} = R\,\bar{\bar{\varepsilon}}\,R^{-1}\,. \tag{7}$$

The full expression for the local rotation is:

$$\theta = \frac{1}{2}\arctan\left(\frac{2\varepsilon_{yy}(b-a)^2(t-1)xf(y)}{\varepsilon_{xx}f(y)^4 - \varepsilon_{yy}(b-a)^2[f(y)+(t-1)x]\,[f(y)-(t-1)x]}\right), \tag{8}$$

with $f(y) = (b - at) + (t - 1)y$.

The $\theta(x, y)$, $\varepsilon_{ii}(x, y)$ and $\varepsilon_{jj}(x, y)$ functions are plotted in Fig. 10 for the same values of (a, b, t) as previously. The permeability distribution is unchanged. On the θ distribution, the existence of a central "optical axis" can be clearly seen. ε_{ii}, ε_{jj} and μ_{zz} show significant gradients over the surface of the lens. However, ε_{ii} and ε_{jj} are on the same order of magnitude as ε_{xx} (positive and close to 0) and ε_{yy} (greater than 1), respectively. Similarly, μ_{zz} is comparable to 1. It should be noted that ε_{jj} diverges for large values of x, particularly when $y \to a$, which limits the lateral extent of the input pattern.

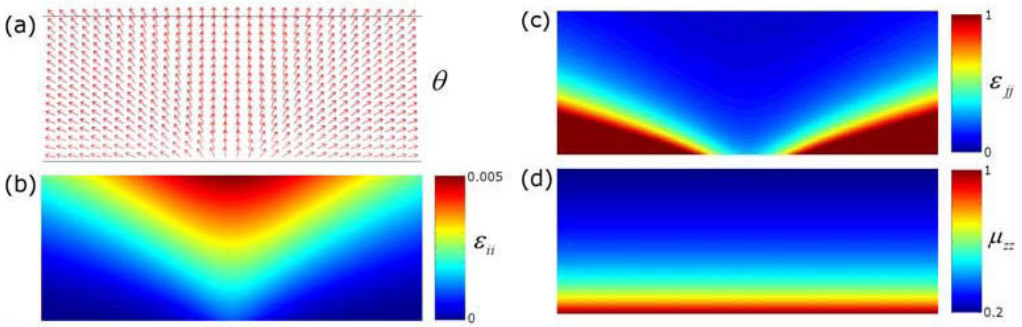

Figure 10: (a) Spatial distribution of the rotation angle of the local coordinate system. The red arrows show the direction of the local j vector, for a discrete set of points. However, the angle is defined at every point inside the homogenous slab. (b-d) Full set of effective parameters inside the flat hyperlens in the local rotated coordinate system (i, j, z)

We introduced those local parameters as material parameters for a slab into a frequency-domain 2D finite element method solver (namely the commercial software COMSOL). The input near-field pattern is simply two very narrow (λ_0/60) sources of magnetic field centered at + and - λ_0/20 and positioned directly at the bottom interface of the lens. The rest of the bottom boundary is a perfect magnetic conductor. Above the lens is placed an air layer. The top and side boundaries are Perfectly Matched Layers. The wavelength in air was chosen to be 7.5 times larger than the thickness of the lens.

Figure 11 shows the resulting magnetic field map (a) and the plot of this field on the input and output boundaries of the lens (b). The distance between the two peaks is multiplied by t (5 here) thanks to the lens. It should be noted that a significant spreading of the peaks can also be observed.

This set of parameters could be implemented by means of individual particles with controlled values of permittivity along two orthogonal directions and a controlled value of permeability along the third. Moreover, each one of them would have to be individually oriented. The

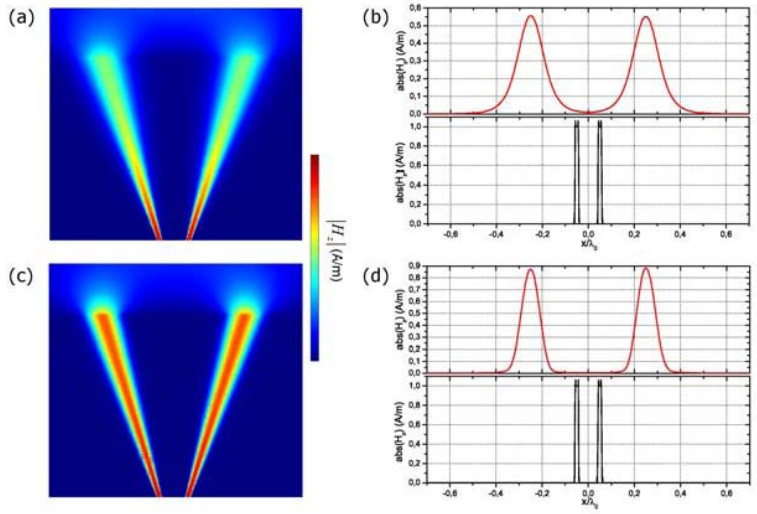

Figure 11: (a) Simulated magnetic field map inside the flat hyperlens following equation (8) and in the air above for an input pattern of two sub-wavelength sources. (b) Corresponding field plot for both interfaces of the lens. (c-d) Same field map and plot for the lens with simplified parameters (constant ε_{ii} and ε_{jj}).

structures presented in the first sections of this paper suggest that the realization of such particles is not completely unrealistic. However, the actual importance of the calculated constraints should be checked. Since we have noted the order of magnitude of the calculated perfect parameters, we can check the effect of dropping all gradients on the local effective parameters in the rotated coordinate system. In other words, we define ε_{ii}=0.001, ε_{jj}=2.5 and μ_{zz}=1 at every points inside the device, with the same $\theta(x, y)$ function as before. Figures 11(c) and 11(d) show the same map and plot of the magnetic field as before but with those simplified material parameters. The magnification effect is still present and the distance between the peaks is unchanged. This means that when a channeling slab is used, the proper orientation of the anisotropy dominates over its specific values in the transformation procedure.

Additionally, it is possible to explore other $\theta(x, y)$ distributions that could perform different functions. Equation (9) (a, b have the same meaning as before and all c_i are constants), for example, allows transforming point-like sources at the input into very large line sources at the output (Figs 12(a-b)). Such a function could be useful in the field of antennas. Equation (10) leads to a concentration of the field along the transverse direction (Fig. 13), which could be interesting in detection systems to focus energy onto a probe.

$$\theta(x, y) = \text{sign}(x) \left[\arctan\left(-c_1(|x| + c_2) \frac{b-a}{b-y} \right) \right] , \tag{9}$$

$$\theta(x, y) = \arctan\left(c_3 \frac{x(-y^2 + (a+b)y - ab)}{(a-b)^2} \right) . \tag{10}$$

In summary, in order to perform a given operation on the field patterns, one can use either a $\theta(x, y)$ function given by a full transformation procedure or simply search for a suitable function directly. The main point to be considered when using the second method is that the propagation

direction inside the lens is dominated by the local j vector. It should be noted that this can lead us back to the cylindrical hyperlens already mentioned: we just have to choose two cylindrical interfaces and then a cylindrical $\theta(x, y)$ function is the most straightforward choice to map the field from the inner to the outer interface [13, 14].

At this point we have only used homogenous simulations to check the validity of our expressions. However, it is possible to implement a micro-structure into our FEM software. In other words, we will replace the locally rotated effective parameters by a metamaterial structure which only uses simple materials arranged into a suitable geometry. Following the previous works on hyperlenses, we can try with a stack of layers of two different materials (of permittivities ε_1 and ε_2). When the layers are of equal thickness, very thin with respect to the wavelength and most importantly normal to the j direction, the effective parameters are directly given by Eq. (11). For example, in order to obtain ε_{ii}=0.001 and ε_{jj}=2.5, we will use layers with permittivities of ε_1=0.001-0.05i and ε_2=0.001+0.05i (the gain comes from the constraint of zero loss for the effective parameters).

$$\begin{cases} \varepsilon_{ii} &= \dfrac{\varepsilon_1 + \varepsilon_2}{2} \\ \varepsilon_{jj} &= \dfrac{2\varepsilon_1\varepsilon_2}{\varepsilon_1 + \varepsilon_2} \end{cases} . \tag{11}$$

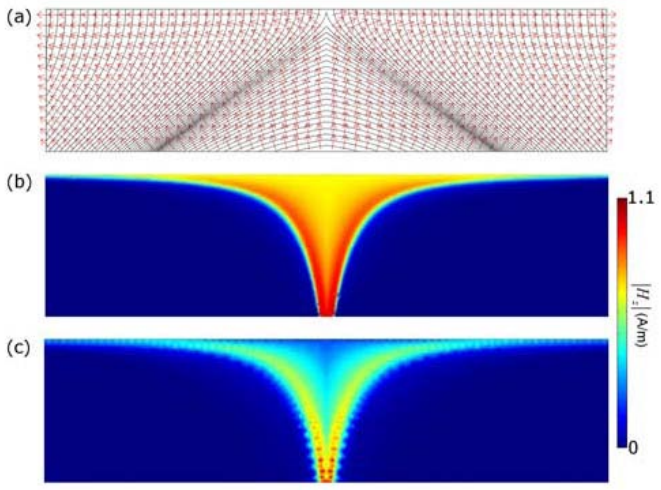

Figure 12: (a) Orientation of vector j for the local rotation given by equation (9) (red arrows). The black curves are the limits of the layers normal to j that can be used to implement the required anisotropy. (b) Magnetic field inside the lens for the homogenous case (b) and the microstructured one, using the layers configuration of (a).

All of the possible layer boundaries form a family of curves that can be found by solving the equation of orthogonality with $j(x, y)$. Among these curves, we can choose any subset that corresponds to reasonable thicknesses with respect to the homogenization conditions. Figure 12(a) shows such a set of curves for the lens that follows Eq. (9). It can be seen that the condition of equal thickness is not globally respected. However, since the gradient on the thickness is small, we can reasonably consider that we have *locally* neighboring layers of approximately

equal thickness. The relevance of this assumption is confirmed by the simulation result for the microstructured slab presented in Figure 12 (c).

Finally it should be noted that most of the calculations were performed for lossless cases. The introduction of losses can significantly deteriorate the performance of hyperlenses. However, the deterioration is strongly dependent to the length of the path inside the device. For instance, the deterioration is very strong when we follow Eq. (9) (Figure 12 shows a lossless case only) whereas it is reasonable for the field concentrator with Eq. (10) (Figure 13 shows a lossy case).

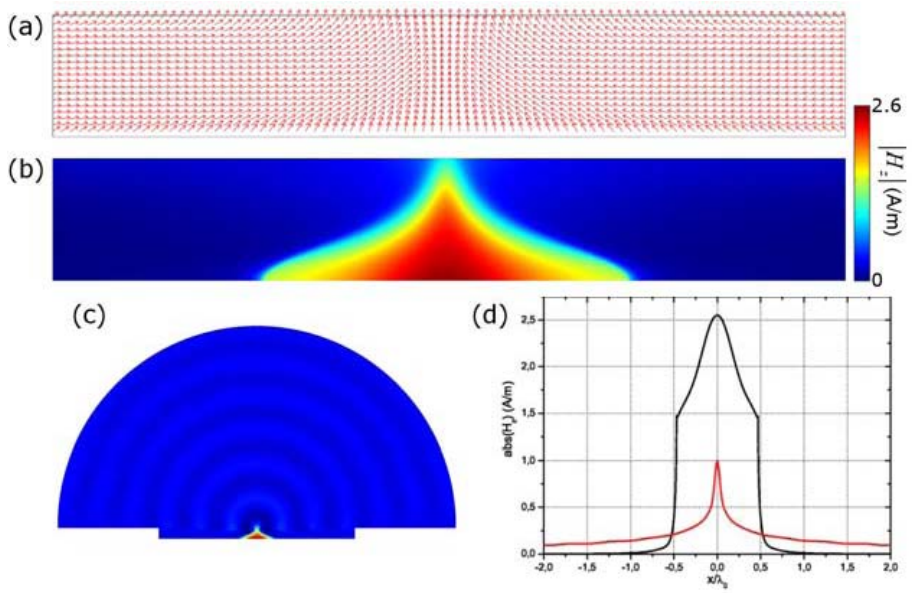

Figure 13: (a) Orientation of vector j for the local rotation given by Eq. (10) (red arrows). Magnetic field inside the lens and in the air above (c) for the homogenous case. (b) Corresponding field plot on both interfaces of the lens, showing concentration of the field along the transverse direction. Unlike the previous cases, this simulation includes losses (loss tangent of 21 and 0.03 for ε_{ii} and ε_{jj} respectively).

6 Conclusions of the Ariadna study

A Full dielectric approach taking advantage of the recent advances in Ferroelectrics technology seems suitable for fabricating a partial transparency cloak at microwaves and Terahertz frequenies. The underlying physics principles which permit one to tailor the effective permeability values are similar to those used for an SRR-cloak operating at microwaves. As a consequence, a high-κ cloak also suffers from the same frequency limitations by showing comparable Lorentz-type dispersion characteristic. Some optimization procedures can be however introduced in order to extend the bandwidth as demonstrated in Fig. 14 which compares various situations. From the fabrication side, the technological challenges are dramatically relaxed when the upper part of the electromagnetic spectrum is targeted. The concept of Magnetic Mie resonance resulting from the light confinement is quite general and could be extended in principle to optics

where metal nanowire arrays were proposed to satisfy the localization [19]. Beyond the search of invisibility which appears as an ultimate goal in the control of light, many applications could be addressed through transformation optics such as lenses. In particular, we demonstrated that hyperlens or high focusing devices can be designed by this procedure having in mind the technological constraints and notably flat interfaces. Such a condition is a requirement in planar deposition techniques such as those used in a full semiconductor technology [20].

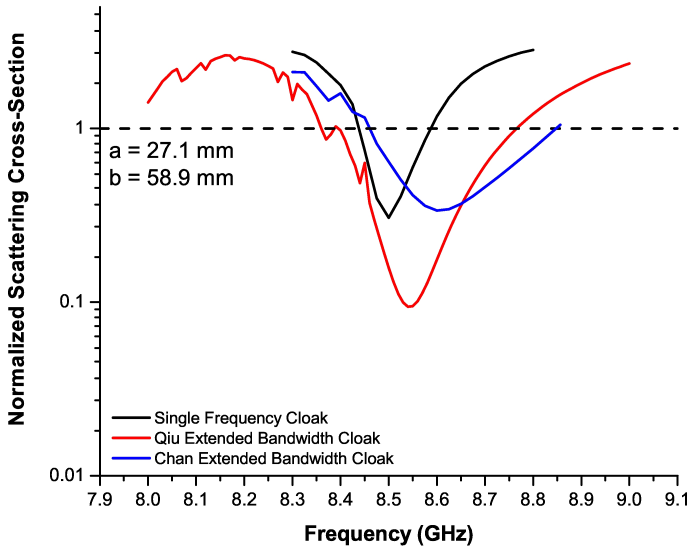

Figure 14: Results of the optimization of an electromagnetic cloak designed for operating around 8 GHz which is based on the extension principles of Chan [21] and Qiu [22].

Acknowledgments

The authors would like to thank Won Park from the University of Boulder (USA) for fruitful discussions along with F. Zhang, currently working at IEMN, and J. Zhou from the University of Tsinghua for their help in the fabrication and the characterization of the BST samples.

References

[1] D. Mittleman, Sensing with Terahertz Radiation (Springer, 2003).

[2] J. D. Joannopoulos, R. D. Meade, and J. N. Winn, Photonic Crystals: Molding the Flow of Light. (Princeton University Press, Princeton, 1995).

[3] U. Leonhardt, Science **312**, 1777-1780 (2006).

[4] J. B. Pendry, D. Shurig, and D. R. Smith, Science **312**, 1780-1782 (2006).

[5] D. Schurig, J. B. Pendry, and D. R. Smith, Opt. Exp. **14** 9794 (2006).

[6] D. Schurig, J. J. Mock, B. J. Justice, S. A. Cummer, J. B. Pendry, A. F. Starr, and D. R. Smith, Science **314**, 977-980 (2006).

[7] W. Cai, U. K. Chettiar, A. V. Kildishev, and V. M. Shalaev, Nature Photonics **1**, 224 - 227 (2007).

[8] S. A. Cummer, B. I. Popa, D. Schurig, D. R. Smith, and J. Pendry, Phys. Rev. E **74**, 36621-36621 (2006).

[9] A. V. Kildishev, and V. M. Shalaev, Optics Lett. **33**, 43 (2008).

[10] D. P. Gaillot, C. Croenne, and D. Lippens, Opt. Exp. **16**, 3986 (2008).

[11] A. Salandrino and N. Engheta, Phys. Rev. B **74**, 075103 (2006).

[12] Z. Jacob, L. V. Alekseyev and E. Narimanov, Opt. Exp. **14**, 8247 (2006).

[13] Z. Liu, H. Lee, Y. Xiong, C. Sun, X. Zhang, Science **315**, 686 (2007).

[14] H. Lee, Z. Liu, Y. Xiong, C. Sun, X. Zhang, Opt. Exp. **15**, 15886 (2007).

[15] S. O'Brien, and J. B. Pendry, J. of Phys. **14**, 4035 (2002).

[16] Q. Zhao, B. Du, L. Kang, H. Zhao, Q. Xie, B. Li, X. Zhang, J. Zhou, L. Li, and Y. Meng, Appl. Phys. Lett. **92**, 051106 (2008).

[17] O. Acher, J.-M. Lerat, and N. Mallejac, Opt. Exp. **15**, 1096-1106 (2007).

[18] D. R. Smith, and J. B. Pendry, J. Opt. Soc. Am. B **23**, 391-403 (2006).

[19] Q. Wu and W. Park, Appl. Phys. Lett. **92**, 153114 (2008).

[20] J. Hoffman, L. Alekseyev, S. S. Howard, K. J. Franz, D. Wasserman, V. Podolskiy, E. E Narimanov, D. L. Sivco, and C. Gmachl, Nature Lett. **946** (2007).

[21] H. Chen, Z. Liang, P. Yao, X. Jiang, H. Ma and C. T. Chan, Phys. Rev. B **76**, 241104 (2007).

[22] M. Yan, Z. Ruan and M. Qiu, Opt. Exp. **15**, 17772 (2007).